




Analyzing the Microwave Absorption Properties of $\text{BaFe}_{12}\text{O}_{19}$, $\text{Ba}_4\text{MnZnFe}_{36}\text{O}_{60}$ and NiFe_2O_4 Particles

MINA MORADNIA,^{1,4} MEHDAD FATHI,^{2,5} MOSTAFA MEHDIPOUR ^{2,6}
and HOOMAN SHOKROLLAHI^{3,7}

1.—Magnetic Materials Research Lab, Department of Materials Engineering, University of Houston, Houston, TX, USA. 2.—Magnetic Materials Research Lab, Department of Materials Engineering, Faculty of Mechanical Engineering, University of Tabriz, Tabriz, Iran. 3.—Electroceramics Group, Department of Materials Science and Engineering, Shiraz University of Technology, Shiraz, Iran. 4.—e-mail: minamoradnia@gmail.com. 5.—e-mail: mehrdadf.t91@gmail.com. 6.—e-mail: Mostafa_mehdipour67@yahoo.com. 7.—e-mail: Shokrollahi@suttech.ac.ir

A stoichiometric ratio of the Merck chlorides of Barium, Iron, nickel and NaOH as an agent was used to obtain the nano-crystalline ferrites ($\text{BaFe}_{12}\text{O}_{19}$, $\text{Ba}_4\text{MnZnFe}_{36}\text{O}_{60}$ and NiFe_2O_4) by a combination of co-precipitation and high-energy reactive milling (RM) methods. After milling, the as-synthesized ferrite materials were exposed to a heat treatment at 1100°C for 4 h with the heating rates of $10^\circ/\text{min}$. After cooling the powders of ferrites inside the furnace, they were sintered at 1200°C for 4 h. The microstructural, structural, magnetic, and microwave absorption features were examined by x-ray diffractometry (XRD), scanning electron spectroscopy (SEM), vibrating-sample magnetometry (VSM) and network analysis (VNA), respectively. As can be seen in the hysteresis loops, both saturation magnetization and coercivity were changed by altering the ferrite kind. After sintering, the Ba-ferrites showed a smaller amount of saturation magnetization of 300 G (0.03 T) and a larger quantity of intrinsic coercivity 1.8 kOe (144 kA/m) compared to the Ni-ferrite and $\text{Ba}_4\text{MnZnFe}_{36}\text{O}_{60}$. After sintering, the samples' reflection loss spectra were changed and reached the maximum value of -35 dB (at resonance frequency) for NiFe_2O_4 , making it suitable for application in the microwave and resonance absorbers.

Key words: Ferromagnetic particles, co-precipitation, sintering, magnetic and microwave absorption properties

INTRODUCTION

A particular kind of environment-related pollution is increasing: the broad application of electromagnetic (EM) waves in wireless communications like EM waves of 0.8–1.2 GHz, which are employed for cell phones, 2.45 GHz for the purpose of electronic ranges, 5.6–8.2 GHz (G-band) for synthetic aperture radar (SAR)^{1,2} or microwave communications on the ground, 8.2–12.4 GHz (X-band) and

12.4–18 (Ku-band) for SAR or electron spin resonance (ESR) equipment. These have caused numerous investigations within the domain of 'microwave absorbing materials' so as to minimize the detrimental impacts of electromagnetic waves upon biological tissues in the shape of electromagnetic interference (EMI), accompanied by their alleged application as radar absorbing material (RAM).³

Nowadays, ferrite materials are widely utilized in electronic devices through the microwave range, and there are currently other fields for application of ferrites such as phase shifters, magneto-optical areas, wireless communications, and surveillance, as well as sensing and tracking fields. Certain

(Received February 5, 2020; accepted July 4, 2020; published online July 20, 2020)

magnetic properties like coercivity and magnetization can effectively change EMI properties.⁴ Ferrites have been classified into three groups according to their crystalline structures: hexa-ferrites, spinels and garnets. Hexa-ferrites and spinel ferrites have been considered as practical materials for adverse microwave absorption applications, and different methods have been used to measure their magnetic characteristics. Selecting representative materials from each of the three crystalline structure groups makes it possible to investigate a wide range of materials, comparing their magnetic properties and absorbing behavior under the same conditions (identical thickness of the samples along with the equal ratio of powder to epoxy (70:30), something that had not really been gathered into one paper before).⁵⁻⁷

There exist six types of hexa-ferrites based on their composition and crystalline structure, including *M*, *W*, *Y*, *Z*, *X* and *U* types.⁸ From the magnetic point of view, the *M*-type is the most reputable hard type. For a long time now, *M*-type barium hexa-ferrite ($\text{BaFe}_{12}\text{O}_{19}$) has received attention as an EM absorber on account of its employment as a dielectric or magnetic filler in the field of electromagnetic attenuation.⁹ The *U*-type hexa-ferrite $\text{Ba}_6\text{Me}_2\text{Fe}_{36}\text{O}_{60}$ (Me = a bivalent transition metal) has the largest unit cell size and the most complex crystal structure among types of hexa-ferrite. The increasing attention to this material is due to its structural complexity and its application in tuned microwave absorbers.^{10,11} Nickel ferrite (NiFe_2O_4), with a cubic spinel shape, is a magnetic material which has been investigated as a microwave absorbing material.¹² Various methods can be used for the synthesis of ferrites, including the solid-state reaction, hydrothermal method, low-temperature combustion, mechanical alloying and co-precipitation.¹³⁻¹⁵ As compared with the other methods, the mixture of high-energy ball milling and co-precipitation methods are cost-effective strategies, appropriate for production in large quantities.⁹ In this strategy, the precipitation is performed through applying a mixed solution of chlorides (Fe, Sr and Zn) to a $\text{NaOH}/\text{Na}_2\text{CO}_3$ solution.¹⁶⁻¹⁹ The carbonates or nitrates of cations can be employed, as well, in lieu of their chlorides for the syntheses of hexa-ferrites.^{20,21} Heat-treatment expedites the process, and hexa-ferrites are crystallized thoroughly in hexagonal pyramidal or plate-like form after they have been cooled in the furnace.^{15,22}

This study shows a comparison between three different particles of nickel ferrite, BaM and MnZnU. Only a few studies have been carried out to determine the MW-absorbing properties of thick films in composite form at X-band frequencies, especially in the complex crystal structure of *U*-type hexa-ferrites.^{23,24}

EXPERIMENTAL METHOD

Praveena and Srinath prepared CoFeO_2O_4 by using cobalt nitrate [$\text{Co}(\text{NO}_3)_2 \cdot 6\text{H}_2\text{O}$] and ferric nitrate [$\text{Fe}(\text{NO}_3)_3 \cdot 9\text{H}_2\text{O}$] solutions taken at the stoichiometric ratio through the Co-precipitation method.²⁵ As in their work, we used a stoichiometric ratio of Merck chlorides of Barium, Iron, nickel and NaOH as an agent to attain nano-crystalline ferrites by the mixture of c-precipitation and high-energy reactive milling (RM) methods. The starting materials were made from high-purity powders (99.99%) and they obtained the co-precipitation route in order to reach as-synthesized materials in accord with Ref.3. They were milled in a regular atmosphere using a Pulverisette 4 (Fritsch) planetary ball mill. Stainless steel vials with a volume of 3000 cm³ and stainless steel balls with a diameter of 20 mm were applied for milling. The mass ratio of the ball to the powder was 12:1. The vial rotational speed (ω) and the disc rotational speed (Ω) were set at 900 rpm and at 500 rpm, respectively, during the whole milling time. After milling for 7h, the as-synthesized materials were exposed to a heat treatment at 1100°C for 4 h at the heating rates of 10°/min. Following the cooling of the ferrite powders inside the furnace, a pressure of 0.1 MPa was applied and they were sintered at 1200°C for 4 h. The sintered specimens were cooled in the furnace and then crushed to provide sintered ferrite powders. The powder was mixed with an appropriate amount of non-viscous epoxy resin using a monotone ultrasonic mixer to avoid any agglomerations. Then, hardener was added to the mixture and it was cast into a tiny PE mold (in the case of the samples prepared for magnetic/MV absorption tests) or it was applied to the surface of the Al plates (in the case of the samples prepared for the pull-off adhesion test). In regard with the former, they were examined visually under a lamp in order to confirm their homogeneity from the top surface to the bottom and to exclude samples with non-consistency in their powder-to-resin homogeneity or samples with trapped air bubbles trapping. In respect to the latter, the only problem was to achieve composite layers with a constant thickness of 2.5 mm. This was fulfilled using a special ruler gliding on the surface of the composite-coated Al plate and adjusting the thickness of the epoxy/powder coating by removing excessive sections. The preparation procedure of the composite samples is summarized in Table. I. Applying the composite on an aluminum surface without conducting any pretreatment on the metallic surface resulted in a pull of strength of 10 MPa, and the failure was mainly in adhesive mode from the Al surface. The anodized Al surface reached 12 MPa, which was mainly cohesive from the composite.

Table I. Preparation procedure of composite samples for the investigation of the magnetic and microwave absorption properties

Type of epoxy	Type of hardener	Time curing	Temperature curing	Time post-curing	Temperature post-curing
Bisphenol A diglycidyl ether (epolam)	Amine hardener	1 h	25°C	24 h	50°C

The phase identification of the synthesized ferrites was carried out by XRD (Siemens, D5000 x-ray diffractometer) via Cu K α radiation ($\lambda = 1.5405 \text{ \AA}$). The morphology of powders was studied by SEM (SEM, Hitachi S4160). The magnetic properties of the samples were specified at room temperature in the field scope of -10 kOe (-800 KA/m) to 10 kOe (800 KA/m) using a magnetometer (Magnet-Physics, C-300). To examine the properties of absorption, entire specimens (70 wt. %) were blended with epoxy resin and 3% hardener. Then, the mixture was placed in a rectangular pellet ($21.7 \times 10 \text{ mm}^2$) with a 2.5 mm thickness and dried at ambient temperature for 24 h.

The provided composite was polished and mounted on aluminum foil (to achieve a metal-backed absorber with a single layer) to be precisely suitable for the measuring waveguide. The reflection loss was measured by a VNA (ST8410-C) in the X-band from 8 to 12 GHz at room temperature.

RESULTS AND DISCUSSION

As can be seen in the XRD patterns in Fig. 1, BaFe₁₂O₁₉ ($2\theta = 34.196^\circ$; JCPDS card no. 00-007-0276) and NiFe₂O₄ ($2\theta = 35.425^\circ$; JCPDS card no. 00-044-1485) were synthesized after sintering. The XRD patterns of Ba₄MnZnFe₃₆O₆₀ were investigated by X-powder software and the results were consistent with the previously stated *U*-type hexa-ferrites XRD patterns.²³ There were no extra peaks related to the other phases. The lattice constant (a) related to the cubic crystal system was obtained via the equation $a = d \sqrt{(h^2 + k^2 + l^2)}$, in which (*h k l*) are the diffraction peak Miller indices and '*d*' pertains to the interplanar spacing.²⁶ By using this equation and the information of Fig. 1, the lattice constant (a and c) for our samples can be studied in Table II.

Micrographs of ferrite powders are shown in Fig. 2. By changing the ferrite type, the particles show numerous morphologies (Fig. 2a-c). The solid-state transformation reaction rate pursuing the Jonhson-Mehl-Avrami (JMA) kinetic model could be implemented as follows:

$$\frac{dx}{dt} = An(1 - \alpha) \left[\ln \frac{1}{(1 - \alpha)^{(n-1)/n} \exp\left(-\frac{E}{RT}\right)} \right]. \quad (1)$$

In this route, α relates to the reacted fraction, t is related to the transformation time, T shows the

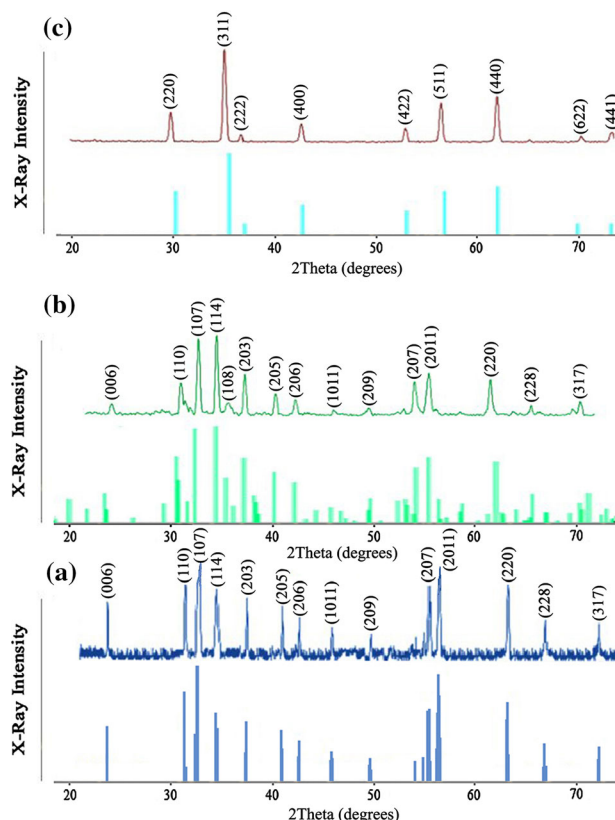


Fig. 1. XRD patterns of particles after sintering (a) Ba₄MnZnFe₃₆O₆₀, (b) BaFe₁₂O₁₉ and (c) NiFe₂O₄.

temperature, R has to do with the gas constant, n pertains to the Avrami index parameter, which is changed by the material type, E and A are the activation energy and the pre-exponential variable. Consequently, the Avrami index factor is altered by changing the ferrite type as the particles' morphology is altered.¹⁷

The combination of high-energy ball milling and co-precipitation methods makes it possible for products to have smaller grain sizes compared to the standard ceramic method; the ferrite kinds synthesized by this process tend to have higher magnetic saturation.¹⁵ The sintered particles' magnetic features are presented in Fig. 3. The saturation magnetization (M_s) proved to be dependent on the ferrite type, rising from 300 G (0.03 T) (for BaFe₁₂O₁₉) to 350 G (0.035 T) (for NiFe₂O₄). The saturation

Table II. Lattice constants of ferrites

Ferrites	BaFe ₁₂ O ₁₉	Ba ₄ MnZnFe ₃₆ O ₆₀	NiFe ₂ O ₄
The lattice constants (a)	5.87(Å)	5.88(Å)	8.41(Å)
The lattice constants (c)	23.2(Å)	113(Å)	8.41(Å)

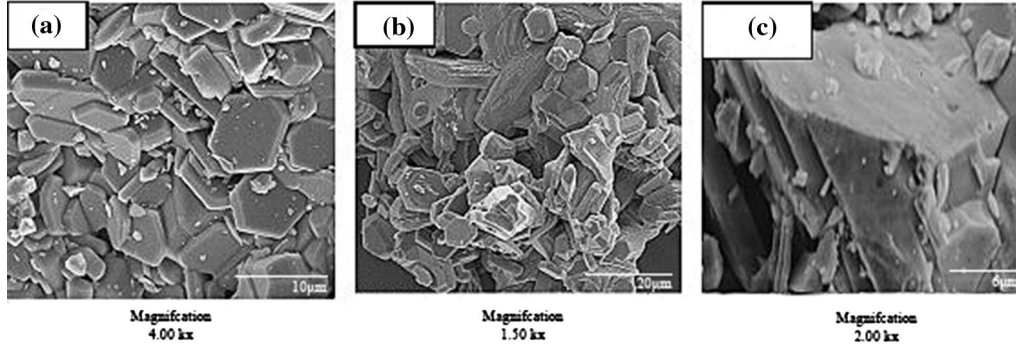


Fig. 2. SEM micrographs of particles heat-treated (after sintering and crushing) at temperature of 1200°C (a) BaFe₁₂O₁₉, (b) Ba₄MnZnFe₃₆O₆₀ and (c) NiFe₂O₄.

magnetization of Ba₄MnZnFe₃₆O₆₀ is between these values and is compatible with Ref.23. Changes in saturation magnetization may be a result of the formation of soft and hard phases, as verified by the x-ray examination of the powder which has been heat-treated at 1200°C (Fig. 1a–c). Morphological change and the average particle size can influence magnetic characteristics as well.^{24,27} The coercivity (H_c) of BaFe₁₂O₁₉ (1.8 kOe) decreases to 0.02 kOe (1.6 kA/m). In comparison with the other similar ferrites, the coercivity of BaM hexa-ferrite is lower, which can result from the effect of sintering,^{7,25} and²⁸ Totally, the coercivity could be ascribed to the magnetization and magneto-crystalline anisotropy by a modified Brown's Equation as in Eq. 2²⁹:

$$H_c = 2 \frac{k}{M_s} \alpha_{\theta} \alpha_{ex} \alpha_k - N_z M_s, \quad (2)$$

in which α_{θ} is related to the grains' orientation distribution (a structure which has been oriented randomly equals 0.5), α_k is the coefficient considering a decline in anisotropy in the area close to the internal surface as grain boundaries and inter-phases and α_{ex} is utilized to depict the impact of the exchange coupling between the adjacent grains in the magnet coercivity field. K and N_z have to do with the magneto-crystalline anisotropy and demagnetization parameters, respectively. By increasing the particle size by sintering, the disordering on the surface of particles can be decreased, and increasing magnetization saturation will appear. Consequently, according to "modified Brown's Equation," by increasing M_s , H_c will be decreased. The Mn–Zn U -type hexa-ferrite has a

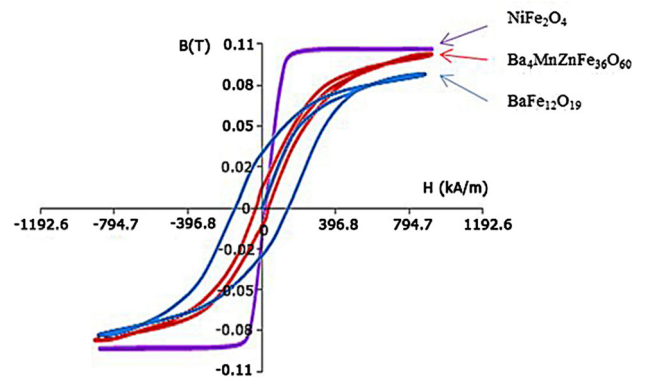


Fig. 3. Effect of the ferrite kind on hysteresis loops of samples after the sintering.

relatively small $H_c = 0.24$ kOe (19.2 kA/m). This ferrite shows acceptable coercivity as compared to Zn₂U and Ni₂U, carried out by Lisjak et al.¹⁵

For comparing the magnetization properties of our ferrites with other similar works, we note that K. Sadhana and his co-workers reached a ratio of (M_r/M_s) in the range of (0.43 to 0.51) for BaFe₁₂O₁₉, which is higher than the ratio of ($M_r/M_s = 0.27$) for BaFe₁₂O₁₉, synthesized through our works. In addition to BaFe₁₂O₁₉, V. Jagadeesha and his co-workers studied the influence of Sm³⁺-Gd³⁺ upon the magnetic characteristics of Mn–Zn ferrites synthesized by the combustion route, and the ratio of (M_r/M_s) was about 0.46. Also, Praveena studied Zn²⁺-substituted MnFe₂O₄, and the ratio of (M_r/M_s) was in the range of (0.4–0.42). Yet the ratio of (M_r/M_s) was about 0.04 for our NiFe₂O₄.^{30–32}

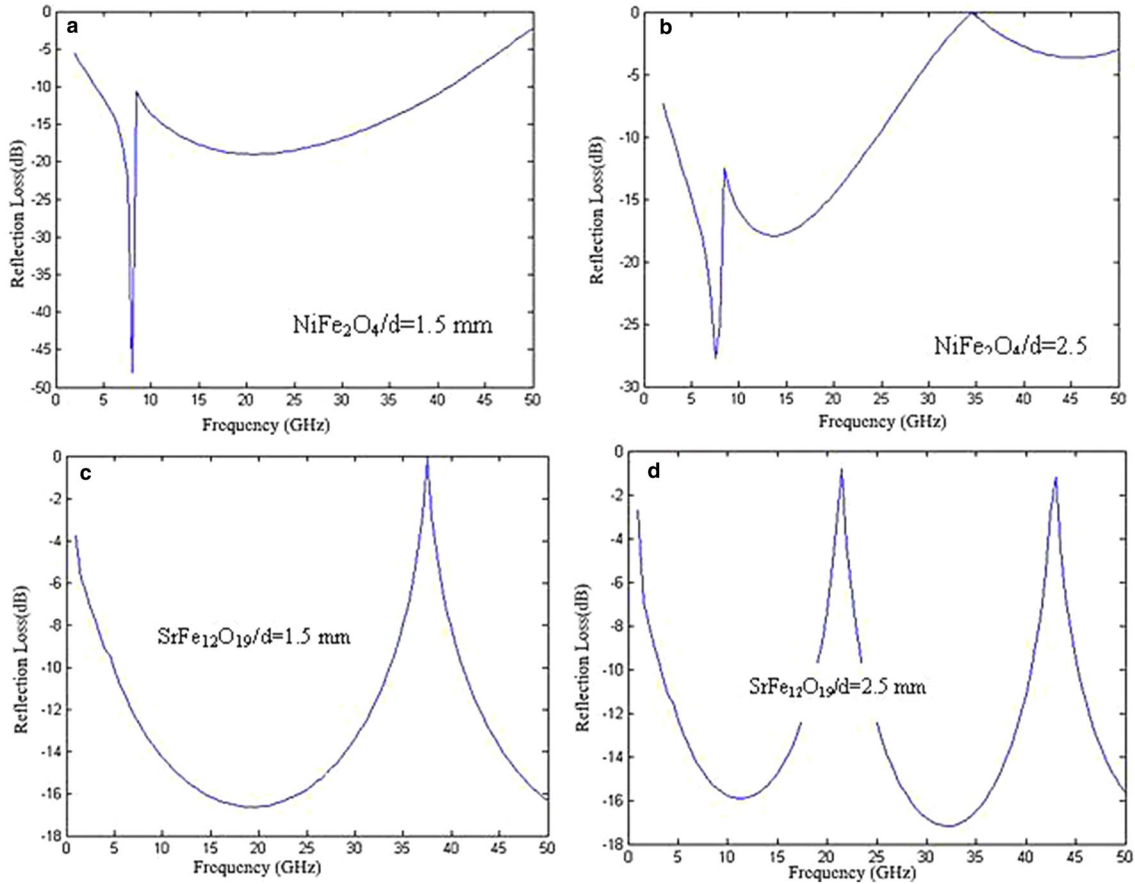


Fig. 4. Simulated reflection loss plots in the frequency range of 0-50 GHz for the synthesized BaFe₁₂O₁₉ and NiFe₂O₄ samples at different thicknesses; (a) NiFe₂O₄/d = 1.5 mm, (b) NiFe₂O₄/d = 2.5 mm, (c) BaFe₁₂O₁₉/d = 1.5 mm and (d) BaFe₁₂O₁₉/d = 2.5 mm.

The electromagnetic radiation reflection loss (RL) as a result of the normal wave incidence at the surface of a single-layer material supported by means of a perfect conductor was calculated through the transmit-line theory using the relative complex permittivity as well as the permeability^{33–35}:

$$RL = 20 \log \left| \frac{Z_{in} - 1}{Z_{in} + 1} \right| \quad (3)$$

$$Z_{in} = \sqrt{\frac{\mu}{\epsilon}} \left[\tanh \left(\frac{2\pi f d}{c} \right) \sqrt{\mu \epsilon} \right], \quad (4)$$

where RL has to do with the ratio of the reflected power to the incident power in dB, Z_{in} relates to the absorber input impedance, d concerns the absorber thickness, and c is the light velocity. Besides, ϵ and μ are related to both permittivity and permeability, respectively.³⁶ According to Eqs. 2 and 3, the simulations in regard to the impact upon the reflection losses for the BaFe₁₂O₁₉ and NiFe₂O₄ specimens, which have hard and soft magnetic features, are depicted in Fig. 4.³⁷

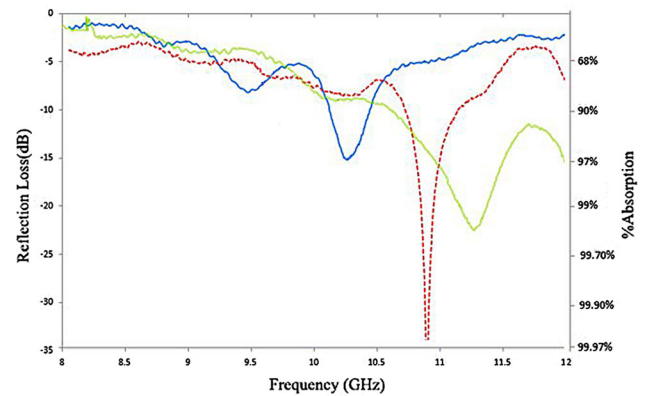


Fig. 5. Changes in (RL) spectra of composite samples made from ferrite powder in the frequency range of 8-12 GHz (a) BaFe₁₂O₁₉, (b) Ba₄MnZnFe₃₆O₆₀ and (c) NiFe₂O₄.

Generally, two types of peak may be derived from the plots. In the two samples a broad, u-shaped peak occurred. This peak was observed for the NiFe₂O₄ sample at 22 GHz for $d = 1.5$ mm and 14 and at 45 GHz for $d = 2.5$ mm. The other peaks kept their consistency by a growth in the thickness observed only in NiFe₂O₄, which is a narrow peak. In order to explain these phenomena properly, the above-

mentioned equations should be reviewed. As to the Eq. 3, there is a periodic relationship between RL and frequency, which can be related to thickness and is reduced by increasing the thickness, which illustrates the effect of thickness as a periodic parameter. The natural resonance frequency could be to do with an intrinsic parameter (like coercivity); it does not have a direct link with thickness. This resonance was seen solely for NiFe_2O_4 , as it is a soft magnetic stage (with a small amount of coercivity resulting in a low level of natural resonance frequency). The synthesized $\text{BaFe}_{12}\text{O}_{19}$ is a hard step; thus, the natural resonance needs to take place at 50 GHz, which is confirmed in the Ref 38.

Figure 5 shows the (RL) spectra of the composite samples made from different kinds of ferrite. It has been observed that RL of the thick film composite specimens changes via altering the ferrite type. In this process, the RL spectra of $\text{BaFe}_{12}\text{O}_{19}$ and $\text{Ba}_4\text{MnZnFe}_{36}\text{O}_{60}$ arrived at -15 dB and -22 dB at resonance frequencies, yet NiFe_2O_4 reached -35 dB at around 11 GHz. The nickel ferrite sample showed more than 65% absorption in almost the whole X-band frequency, even though H. Bayrakdar attained maximum reflection loss with a bandwidth of approximately 2 GHz for ferrite-paraffin polymer composites.³⁹ In comparison with Dimri et al., who obtained the best reflection loss in the 5 mm composite sample, our research on Mn-ZnU ($\text{Ba}_4\text{MnZnFe}_{36}\text{O}_{60}$) hexa-ferrite had a relatively better result in the thick composite film for the sample thickness of 2.5 mm.⁴⁰ Regarding the fact that $\text{Ba}_4\text{MnZnFe}_{36}\text{O}_{60}$ has good absorption properties in the whole X-band, it is useful for minimizing the detrimental impact of electromagnetic (EM) waves upon biological tissues in radar cross-section reduction (RCS) form.²² It can be said that these samples are appropriate for electromagnetic applications and EMI shielding characteristics.^{11,41,42} These changes in RL (Fig. 5) could also be accounted for by a reduction in the coercivity and a rise in the saturation magnetization for ferrite particles based upon the ferromagnetic resonance and transmit-line theories. Changing the magnetic properties of materials altered their permeability, and therefore their absorption properties were changed (by applying Eqs. 1 and 2).

CONCLUSION

Uniform hexagonal plate and pyramidal particles ($\text{BaFe}_{12}\text{O}_{19}$, $\text{Ba}_4\text{MnZnFe}_{36}\text{O}_{60}$ and NiFe_2O_4) were synthesized effectively through a combination of c-precipitation and high-energy reactive milling (RM) methods. Following the sintering process, the Ba-ferrite pure particles exhibited lower saturation magnetization of 300 G (0.03 T) and higher intrinsic coercivity (1.8 kOe) (144 KA/m) in comparison to Ni-ferrite and $\text{Ba}_4\text{MnZnFe}_{36}\text{O}_{60}$. Investigating the microwave absorption properties reveals that the optimum conditions took place for NiFe_2O_4 . The

samples' reflection loss spectra were changed and reached the maximum value of -35 dB (at the resonance frequency) for NiFe_2O_4 , making it suitable for application in microwave and resonance absorbers.

CONFLICT OF INTEREST

The authors declare no conflicts of interest.

REFERENCES

1. Y. Zhang, C. Liu, X. Zhao, M. Yao, and F. Xu, *J. Magn. Mater.* 49415, 29 (2020).
2. K. Qian, Z. Yao, H. Lin, J. Zhou, and X. Guo, *Ceram. Int.* 46, 14 (2020).
3. D. Li, T. Horikawa, J. Liu, M. Itoh, and K. Machida, *J Alloys Compd.* 408, 74 (2006).
4. K. Sadhana, S. Remana, and K. Praveena, *Mater. Sci. Semicond. Proc.* 34, 305 (2015).
5. K. Praveena and S. Srinath, *J. Magn. Magn. Matter* 349, 45 (2014).
6. Y. Yuan, S. Wei, Y. Liang, and X. Wang, *J. Magn. Magn. Matter.* 50, 69 (2020).
7. C. Lei and Y. Du, *J. Alloys Compd.* 82, 144 (2020).
8. B. Cullity and C. Graham, *Introduction to Magnetic Materials*, 2nd ed. (New York: Wiley, 2009).
9. S. Tyagi, H. Baskey, R. Agarwala, V. Agarwala, and T. Shami, *J. Electron. Mater.* 40, 124 (2011).
10. R. Meena, S. Bhattachya, and R. Chatterjee, *J. Magn. Magn. Mater.* 322, 61 (2010).
11. R. Meena, S. Bhattachya, and R. Chatterjee, *Magn. Magn. Mater.* 31, 120 (2010).
12. S. Tyagi, H. Baskey, R. Agarwala, V. Agrwala, and T. Shami, *J. Ceram. Int.* 37, 51 (2011).
13. M. Mehdipour, M. Fathi, S. Ariae, and H. Shokrollahi, *J. Electron. Mater.* 48, 25 (2019).
14. M. Fathi, M. Mehdipour, and H. Shokrollahi, *J. Aust. Ceram. Soc.* 56, 1 (2020).
15. R.C. Pullar, *Prog. Mater Sci.* 57, 133 (2012).
16. H. Hsiang and R. Yao, *Mater. Chem. Phys.* 104, 85 (2007).
17. R. Layer, R. Desia, and R. Upadhyay, *Indian J. Pure Appl. Phys.* 47, 11 (2009).
18. S. Janasi, M. Emurea, F. Landgraf, and D. Rodrigues, *J. Magn. Magn. Mater.* 238, 168 (2002).
19. S. Saloomeh, A. Meibod, P. Pourafshary, and H.R.M. Hosseini, *World Acad. Sci. Eng. Technol.* 4, 77 (2010).
20. M. Bradiceanu, P. Vlazan, S. Novaconi, I. Grozescu, and P. Barvinchi, *Incemc* 56, 181 (2007).
21. A. Texira, T. Ogasawara, and M. Nobrega, *Mat. Res.* 9, 101 (2006).
22. S. Tyagi, R. Agarwala, and V. Agarwala, *Int. J. Mater. Sci.* 4, 93 (2009).
23. R.S. Meena, S. Bhattachrya, and R. Chatterjee, *J. Magn. Magn. Mater.* 322, 65 (2011).
24. S. Padhy, S. Sanyal, R.S. Meena, R. Chatterjee, A. Bose, and I.E.T. Microwaves, *Antennas Propag.* 8, 154 (2012).
25. K. Praveena and S. Srinath, *J. Nanosci. Nanotech.* 14, 4371 (2014).
26. K. Praveena, K. Sadhana, H. Liu, and S. Murthy, *J. Mater. Sci.: Mater. Electron.* 27, 12680 (2016).
27. M. Rangolia, M. Chhantbar, A. Tanna, K. Modi, G. Balda, and H. HJosi, *Indian J. Pure Appl. Phys.* 46, 576 (2008).
28. R.C.O'. Handley, *Modern Magnetic Materials: Principles and Applications* (New York: Wiley, 1999).
29. D. Lisjak and M. Drogenik, *J. Magn. Magn. Mater.* 272, 1817 (2004).
30. K. Sadhana, K. Praveena, S. Matteppanavar, and B. Angad, *Appl. Nanosci.* 2, 247 (2012).
31. K. Praveena, H. Chen, H. Liu, K. Sadhana, S. Murthy, and J. Magn, *Magn. Mater* 10, 1016 (2016).
32. V. Jagadeesha, B. Rudraswamy, K. Sadhana, S. Murthy and K. Praveena, *J. Alloy Compd.* 656, 510–517 (2016).

33. X. Meng, Y. Wan, Q. Li, J. Wang, and H. Luo, *Appl. Surf. Sci.* 257, 455 (2011).
34. L. Xi, X.N. Shi, Z. Wang, Y.L. Zuo, and J.H. Du, *Phys. B: Condens. Matter.* 406, 92 (2011).
35. H. Bertorello, P. Bercoff, and M. Oliva, *J. Magn. Magn. Mater.* 269, 199 (2004).
36. Ü. Özgür, Y. Alivov, and H. Morkoc, Microwave ferrites, part 1: fundamental properties. *J. Mater. Sci.: Mater. Electron.* 20, 221 (2009).
37. E. Hosseinkhani, M. Mehdipour, and H. Shokrollahi, *J. Electron. Mater.* 3, 66 (2013).
38. M. Hurben and C. Patton, *J. Appl. Phys.* 83, 2551 (1998).
39. H. Bayrakdar, *J. Magn. Magn. Mater.* 323, 332 (2011).
40. M.C. Dimri, S.C. Kashyap, and D.C. Dube, *IEEE Trans. Magn.* 42, 589 (2006).
41. S.S. Kim, S.B. Jo, K.I. Gueon, K.K. Choi, J.M. Kim, and K.S. Chum, *IEEE Trans. Magn.* 27, 142 (1991).
42. R. Kaur and G.D. Aul, *Int. J. Sci. Res.* 3, 1069, 229 (2014).

Publisher's Note Springer Nature remains neutral with regard to jurisdictional claims in published maps and institutional affiliations.